ACS APPLIED MATERIALS & INTERFACES

Research Article

www.acsami.org

Enhancing the Performances of P3HT:PCBM–MoS_3-Based H_2-Evolving Photocathodes with Interfacial Layers

Tiphaine Bourgeteau,[†] Denis Tondelier,[‡] Bernard Geffroy,[†,‡] Romain Brisse,[†] Renaud Cornut,[†] Vincent Artero,[§] and Bruno Jousselme*[,†]

[†]Laboratory of Innovation in Surface Chemistry and Nanosciences (LICSEN), CEA Saclay, IRAMIS, NIMBE/UMR3685, Gif-sur-Yvette, Cedex F-91191, France

[‡]Laboratoire de Physique des Interfaces et Couches Minces (LPICM), CNRS UMR 7647, Ecole Polytechnique, Palaiseau F-91128, France

[§]Laboratoire de Chimie et Biologie des Métaux, Université Grenoble Alpes, CNRS, CEA Life Science Division, 17 rue des Martyrs, Grenoble F-38000, France

Supporting Information

ABSTRACT: Organic semiconductors have great potential for producing hydrogen in a durable and economically viable manner because they rely on readily available materials and can be solution-processed over large areas. With the objective of building efficient hybrid organic–inorganic photoelectrochemical cells, we combined a noble-metal-free and solution-processable catalyst for proton reduction, MoS_3, and a poly(3-hexylthiophene):phenyl-C_{61}-butyric acid methyl ester (P3HT:PCBM) bulk heterojunction (BHJ). Different interfacial layers were investigated to improve the charge transfer between P3HT:PCBM and MoS_3. Metallic Al/Ti interfacial layers led to an increase of the photocurrent by up to 8 mA cm^{-2} at reversible hydrogen electrode (RHE) potential with a 0.6 V anodic shift of the H_2 evolution reaction onset potential, a value close to the open-circuit potential of the P3HT:PCBM solar cell. A 50-nm-thick C_{60} layer also works as an interfacial layer, with a current density reaching 1 mA cm^{-2} at the RHE potential. Moreover, two recently highlighted[1] figures-of-merit, measuring the ratio of power saved, $\Phi_{saved,ideal}$ and $\Phi_{saved,NPAC}$, were evaluated and discussed to compare the performances of various photocathodes assessed in a three-electrode configuration. $\Phi_{saved,ideal}$ and $\Phi_{saved,NPAC}$ use the RHE and a nonphotoactive electrode with an identical catalyst as the dark electrode, respectively. They provide different information especially for differentiation of the roles of the photogenerating layer and catalyst. The best results were obtained with the Al/Ti metallic interlayer, with $\Phi_{saved,ideal}$ and $\Phi_{saved,NPAC}$ reaching 0.64% and 2.05%, respectively.

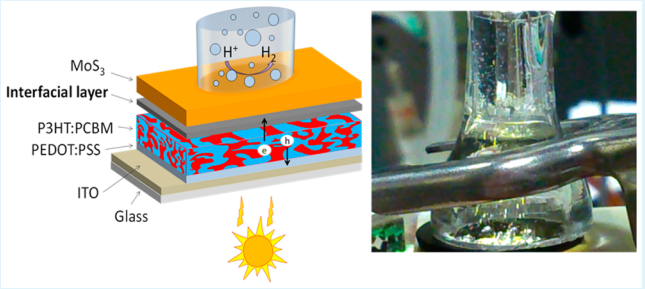

KEYWORDS: *organic photovoltaics, photocathode, H_2 evolution reaction, organic semiconductor, photocatalysis, molybdenum sulfide*

1. INTRODUCTION

Solar-to-chemical energy conversion is an attractive solution for the wide-scale storage and on-demand use of solar energy. Directly producing hydrogen from solar energy and water additionally participates in the building of a carbon-neutral economy. Although benchmarking with fossil-resource-based technologies is still challenging, the search for cost-effective and efficient photocatalytic systems is becoming more and more important.

Photoelectrochemical (PEC) cells performing solar water splitting are widely reported in the literature, both in academic journals[2,3] and in patents.[4] They can have many different configurations depending on the absorber, catalysts, and cocatalysts, number of photoelectrodes, buried junctions, etc.[2,5] An ideal PEC device should meet several criteria:[6] optical absorption in the IR–visible range (corresponding to 80% of the solar flux), resistance to corrosion in aqueous electrolytes, solar-to-hydrogen (STH) conversion yield higher than 10%, competitive cost on an energy-equivalent basis, absence of toxic effects, simple fabrication processes, and great availability of materials.[7] Performant devices exist, such as the AlGaAs/Si/RuO_2/Pt cell, reaching over 18% of solar-to-chemical energy conversion.[8] To reduce the cost linked to the use of expensive and rare materials, multijunction silicon solar cells were used with earth-abundant catalysts by Rocheleau et al.,[9] Suzuki et al.,[10] and Nocera et al.,[11] reaching 7.8% (wired configuration), 2.5% (wireless configuration), and 4.7% (wired configuration and 2.5% wireless configuration), respectively. Besides, cost-effective crystalline metal oxide semiconductors such as Cu_2O[12,13] or

Received: April 23, 2015
Accepted: July 7, 2015
Published: July 7, 2015

DOI: 10.1021/acsami.5b03532
ACS Appl. Mater. Interfaces 2015, 7, 16395–16403

$BiVO_4$[14,15] have been used to build PEC cells other than the above-mentioned systems, with promising STH efficiencies.

Organic semiconductors (OSCs) such as conducting polymers or fullerene derivatives are promising in the field of photovoltaic cells, which now display over 10% power conversion efficiency (PCE)[16] using abundant materials and low-cost processes. An advantage of using OSCs in PEC devices is that, thanks to chemical synthesis, a wide variety of materials can be obtained with different energy levels, which can be tuned to the redox potentials required by water-splitting catalysts to operate. OSCs have thus been used for solar water-splitting devices in different configurations. In a photovoltaic (PV)-electrolyzer configuration, an all-solution-processed triple junction polymer solar cell with an open-circuit potential (V_{OC}) of 2.33 V was connected to an electrolyzer to perform water splitting.[17] In a distinct approach, integrated photocathodes were built based on OSCs such as polyaniline, polypyrrole, poly(3-methylthiophene), or poly(3-hexylthiophene) (P3HT), but only a few microampere per square centimeter photocurrent was obtained in aqueous environment, and the production of hydrogen was not always evidenced.[18−22] Then, when a fullerene acceptor was added to P3HT to form a P3HT:phenyl-C_{61}-butyric acid methyl ester (PCBM) bulk heterojunction (BHJ), this photocathode was used with NaCl as a sacrificial donor, in a two-electrode configuration and still without catalyst, and reached a peak current of 100 nA cm^{-2}.[6] To enhance proton reduction at the photocathode surface, a platinum catalyst was added at the top of an evaporated small-molecule (phthalocyanine/fullerene) p/n planar junction and generated 800 μA cm^{-2} photocurrent corresponding to H_2 evolution from aqueous solution.[23] Recently, molybdenum sulfide (MoS_x) was used as both the acceptor and catalyst in a nanocomposite polypyrrole−Ru/MoS_x photocathode and delivered around 40 μA cm^{-2} at the reversible hydrogen electrode (RHE) potential.[24] In an earlier work, we studied a photocathode based on the photosensitization of a nonprecious catalyst, MoS_3, by a P3HT:PCBM BHJ in aqueous media.[25] MoS_3 was chosen because it is a noble-metal-free H_2 evolution catalyst (with an overpotential of 150 mV[26]) and it can be solution-processed directly onto thin OSC films without thermal treatment, which could be detrimental to the organic layer. In this way, MoS_3 photoproduced hydrogen with a current density of 180 μA cm^{-2} at the RHE potential. Another PEC cell based on a P3HT:PCBM photocathode was recently reported to produce hydrogen from a HCl-acidified acetonitrile solution with a cobaloxime catalyst, with 1 mA cm^{-2} photocurrent density.[27]

In this work, we decided to investigate the possibility of enhancing the performance in aqueous media of our system[25] through the introduction of a dense and conductive layer between the P3HT:PCBM layer and the MoS_3 catalyst. We report here on the results obtained with two different interfacial layers: (1) a metallic material used to improve electronic collection and electronic transfer to the catalyst and (2) a nanocarbon layer used as a fully organic interfacial layer. These two interfacial layers showed improved charge transfer compared to the initial cells without interfacial layers, as evidenced by the ratio of power saved under operation quantified through the determination of the ratiometric power-saved figures-of-merit $\Phi_{saved,ideal}$ and $\Phi_{saved,NPAC}$, as recently proposed by Lewis and coworkers.[1]

2. EXPERIMENTAL SECTION

2.1. Chemicals and Reagents. All manipulations were carried out under an inert argon atmosphere in a glovebox unless otherwise mentioned. Poly(3,4-ethylenedioxythiophene):poly(styrenesulfonate) (PEDOT:PSS; AI 4083 for spin-coated devices) and P3HT (M104; RR = 96.3%) were purchased from Ossila. PCBM was purchased from Solenn BV. Indium−tin oxide (ITO)-coated glass substrates (XY20s) were purchased from Xinyan Technology Ltd. The MoS_3 nanoparticle suspension was prepared according to the literature,[28] and a detailed procedure is given in the Supporting Information (SI).

2.2. Fabrication of Photocathodes. *ITO/PEDOT:PSS/P3HT:PCBM.* The P3HT:PCBM solution was prepared by dissolving 25 mg of P3HT and 25 mg of PCBM in 1 mL of anhydrous *o*-dichlorobenzene in the glovebox. The solution was stirred at 50 °C for 2 h and then at room temperature overnight. PEDOT:PSS was filtered with a poly(vinylidene difluoride) (PVDF) filter (0.45 μm) and spin-coated on a cleaned (see the SI) ITO-coated glass substrate in air (speed: 3000 rpm/ramp: 5 s/dwelling time: 30 s followed by 5000 rpm/5 s/30 s), resulting in a 40-nm-thick layer (measured by profilometry). After thermal treatment in air for 10 min at 150 °C, the substrate was quickly transferred to the glovebox. The P3HT:PCBM blend was filtered with a 0.45 μm PVDF filter and spin-coated on top of the PEDOT:PSS layer (1500 rpm/5 s/60 s). The thickness of the P3HT:PCBM layer was estimated by profilometry at 170 ± 10 nm. Annealing was performed at this stage depending on the deposition of the following interfacial layer.

ITO/PEDOT:PSS/P3HT:PCBM/LiF/Al/Ti−MoS_3. The former electrode was annealed at 140 °C for 5 min in the glovebox and 1.2 nm of LiF followed by 100 nm of Al were deposited under vacuum (<10^{-6} mbar; 0.4 Å s^{-1} for LiF; 0.15 nm s^{-1} for Al) in a Joule evaporator. A total of 30−50 nm of Ti was then evaporated (0.5 Å s^{-1}). The electrode temperature was close to room temperature and, in all cases, below the annealing temperature used to stabilize the BHJ. In the glovebox, the MoS_3 solution was spin-coated at 2000 rpm/5 s/30 s followed by 20 s at 70 °C to dry the remaining solvent. The thickness of the MoS_3 film was 30 nm (measured by profilometry). ITO/PEDOT:PSS/P3HT:PCBM/Ti−MoS_3 and ITO/PEDOT:PSS/P3HT:PCBM/LiF/Al−MoS_3 were prepared in the same way, with only evaporation of Ti or LiF/Al, respectively. As a reference sample, ITO/PEDOT:PSS/P3HT:PCBM/LiF/Al/Ti−Pt/C photocathodes were made with a Pt/C ink. The ink was prepared by sonicating (1 h) 10 mg of commercial Pt/C (Alfa Aesar, 40 wt % of Pt, HiSPEC 4000) in 400 μL of ethanol, 100 μL of deionized water, and 65 μL of a Nafion dispersion [D-520, 5% (w/w) in water and isopropyl alcohol, from Alfa Aesar]. The Pt/C ink was spin-coated under the same conditions as the MoS_3 suspension.

ITO/PEDOT:PSS/P3HT:PCBM/C_{60}−MoS_3. P3HT:PCBM deposited on ITO/PEDOT:PSS was annealed at 140 °C for 5 min in the glovebox. C_{60} (50 nm) was evaporated in a Joule evaporator under vacuum (<10^{-6} mbar; 0.5 Å s^{-1}; 500−530 °C). The MoS_3 catalytic layer was sprayed on top of the heated (85 °C; cf. the SI) solar cell in the air, and the electrode was quickly retransferred into the glovebox.

2.3. Electrochemical and PEC Characterization. Electrochemical measurements were recorded using a BioLogic model VSP potentiostat. A three-electrode configuration was used. For polarization and electrolysis measurements, a glassy carbon plate and an Ag/AgCl (3.5 M KCl) electrode were used as the auxiliary and reference electrodes, respectively. Potentials are quoted against the RHE. Details of the calibration method for the reference electrode are given in SI.

For the photocatalytic tests, the photocathode was not entirely plunged into the electrolyte (0.5 M H_2SO_4): only the MoS_3 side was put in contact with the electrolyte thanks to a rubber seal with a hole corresponding to the electrochemical area. The glass/ITO side was illuminated with a lamp, as presented in Figure S1 in the SI. The samples were illuminated with a 200 W Hg−Xe lamp operated at 106 W coupled with a Spectra-Physics 59472 UV cutoff filter (λ > 440 nm) and a circular mask. Irradiance at the substrate surface was measured to ∼100 mW cm^{-2} thanks to a Coherent PowerMax-USB PM150-50C power sensor.

2.4. Other Methods of Characterization. The current−voltage (J−V) characteristics of organic photovoltaic cells were independently

DOI: 10.1021/acsami.5b03532
ACS Appl. Mater. Interfaces 2015, 7, 16395−16403

measured with a Keithley 2635 system source meter under a nitrogen atmosphere. They were deposited onto an ITO-coated substrate with an etched side for the cathodic contact. A LiF/Al cathode (0.28 cm^2) was deposited under vacuum in a Joule evaporator (<10^{-6} mbar; 0.4 Å s^{-1} for 1.2 nm LiF and 0.15 nm s^{-1} for 100 nm Al). Solar cell performances were characterized under a light intensity of AM 1.5 illumination with an Atlas Solar Constant 575PV simulator. The samples were illuminated through the glass substrate.

3. RESULTS AND DISCUSSION

The effect of interlayers between the MoS_3 catalyst and P3HT:PCBM BHJ on the photocatalytic performance is investigated by studying the photocurrent and photovoltage of the different photocathodes. They are also compared with the electrocatalytic activity of the bare catalyst, MoS_3, which is an inorganic noble-metal-free catalyst for the H_2 evolution reaction (HER), with a 150 mV onset overpotential.[26]

3.1. Increase of the Electronic Transfer at the P3HT:PCBM−MoS_3 Interface with Metallic Interlayers. In order to improve the current density previously obtained with ITO/PEDOT:PSS/P3HT:PCBM−MoS_3 in aqueous electrolyte,[25] we decided to use a LiF/Al layer intercalated between P3HT:PCBM and MoS_3. LiF/Al is widely used as a cathode material for organic solar cells because it has a suitable work function that efficiently collects the electrons from the fullerene derivative acceptor. It consists of a thin LiF layer (1.2 nm) and a metallic Al layer (typically 100 nm) evaporated under vacuum onto the P3HT:PCBM BHJ. When such a solar cell is characterized, the voltage is applied between this Al cathode and the ITO anode. The constructions with ITO/PEDOT:PSS/P3HT:PCBM/LiF/Al−MoS_3 architectures did however not exhibit promising properties because the Al layer was rapidly oxidized in the acidic electrolyte despite the presence of the spin-coated catalyst overlayer. Such an oxidative process was evidenced by the observation of anodic dark currents, which could not be completely reversed even under illumination (Figure S2 in the SI). In other words, the cathodic photocurrent corresponding to H_2 evolution was always found to be lower than the oxidation dark current. Using a mixed MoS_3/TiO_2 catalyst, as described in our previous work, thicker catalyst films were deposited to achieve better protection of the Al layer. In that case, the photocurrent (Figure S2 in the SI; about 0.8 mA cm^{-2}) was significantly higher than the dark oxidation current (about 0.2 mA cm^{-2}). Nevertheless, the performances were not stable with time, and continuous operation resulted in a concomitant decrease of the photocurrent and an increase of the dark current as the Al layer progressively dissolved in the acidic media.

To protect the Al layer, a metallic Ti layer was evaporated on top of Al. Ti had already been used as a protective layer in a Si-based photocathode.[29−32] Organic photocathodes with a Ti overlayer were fabricated starting from ITO/PEDOT:PSS/P3HT:PCBM/LiF/Al by depositing a 30-nm-thick Ti layer in a Joule evaporator. The voltammogram recorded in a 0.5 M H_2SO_4 electrolyte under chopped illumination is presented in Figure 1, with the $J-V$ curve of the equivalent solar cell for comparison.

The performances of the photoelectrodes were significantly improved compared to our previous devices,[25] with a photocurrent value of 8 mA cm^{-2} at 0 V versus RHE and reaching 10 mA cm^{-2} at more cathodic potentials. The onset of light-driven HER (values were taken at 0.1 mA cm^{-2}) was observed at +0.48 V versus RHE. A dark HER onset was found at −0.15 V versus RHE (black dashed line in Figure 1), as expected for MoS_3 under these conditions.[28] The light-driven anodic shift of the HER

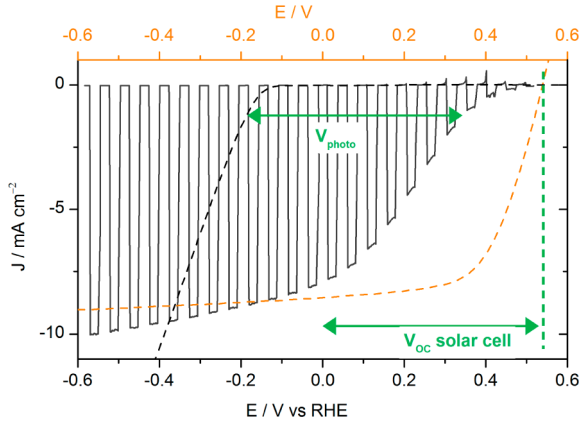

Figure 1. Voltammogram recorded at 50 mV s^{-1} in 0.5 M H_2SO_4 with chopped visible light for an ITO/PEDOT:PSS/P3HT:PCBM/LiF/Al/Ti−MoS_3 photocathode (black line, electrode area 0.32 cm^2) and recorded at 5 mV s^{-1} in 0.5 M H_2SO_4 for an ITO−MoS_3 cathode (black dashed line, electrode area 0.28 cm^2). Potentials are referred to the RHE (bottom axis). The current−voltage curve of an ITO/PEDOT:PSS/P3HT:PCBM/LiF/Al solar cell (orange dashed line, top axis) is shown for comparison.

onset potential, called photovoltage V_{photo} in the following, was thus found to be equal to 0.63 V, close to the open-circuit voltage (V_{OC}) of the organic solar cell (approximately 0.6 V). For illuminated photoelectrodes, current limitation occurs at quite negative potentials, which contrasts with the behavior of electrodes based on a MoS_3 electrocatalyst alone, the $I-V$ curve of which continues to increase with decreasing potential. This plateau (typically 10 mA cm^{-2}) thus does not correspond to a diffusion-limited current. It likely originates from saturation of the solar cell, as observed in typical current−voltage solar cell characteristics shown in Figure 1. To verify this hypothesis, the power of the light source was changed. As shown in Figure 2a, the saturation current changed accordingly. This confirms that the photocurrent value at low potential is limited by the photocurrent produced by the organic solar cell. Moreover, in the range of 0 to 0.5 V, the $I-V$ curve of the photocathode was shifted by approximately 150 mV compared to the solar cell. This value seems to correspond to the overpotential requirement of the MoS_3 catalyst. In order to further investigate this matter, Figure 2b shows the electrochemical and PEC HER activities of the unsensitized and OSC-sensitized MoS_3 and Pt/C catalysts. Similar to MoS_3, the voltammogram of the illuminated ITO/PEDOT:PSS/P3HT:PCBM/LiF/Al/Ti−Pt/C photocathode was anodically shifted by a photovoltage close to V_{OC} of the solar cell (i.e., approximately 0.6 V) compared to the voltammogram of the ITO−Pt/C cathode. The difference of onset potentials of both MoS_3 and Pt catalysts was reflected in the difference of onset potentials of the two photocathodes. Parts a and b of Figure 2 thus show that both the photocurrent and photovoltage are optimal with the LiF/Al/Ti interlayer.

Despite the satisfying performance of the photocathodes, the photocurrent decreased under operation (Figure S3 in the SI). This was attributed to the fact that the electrolyte could reach the Al layer through the Ti layer, resulting in lift-off of the LiF/Al/Ti−MoS_3 metallic layer, as observed during the experiment. To avoid this phenomenon, photocathodes were made without the LiF/Al layer.

As shown in Figure 3, the photocurrent displayed by the photocathode without LiF/Al (blue curve) was similar in intensity to that measured on the photocathode with LiF/Al/

DOI: 10.1021/acsami.5b03532
ACS Appl. Mater. Interfaces 2015, 7, 16395−16403

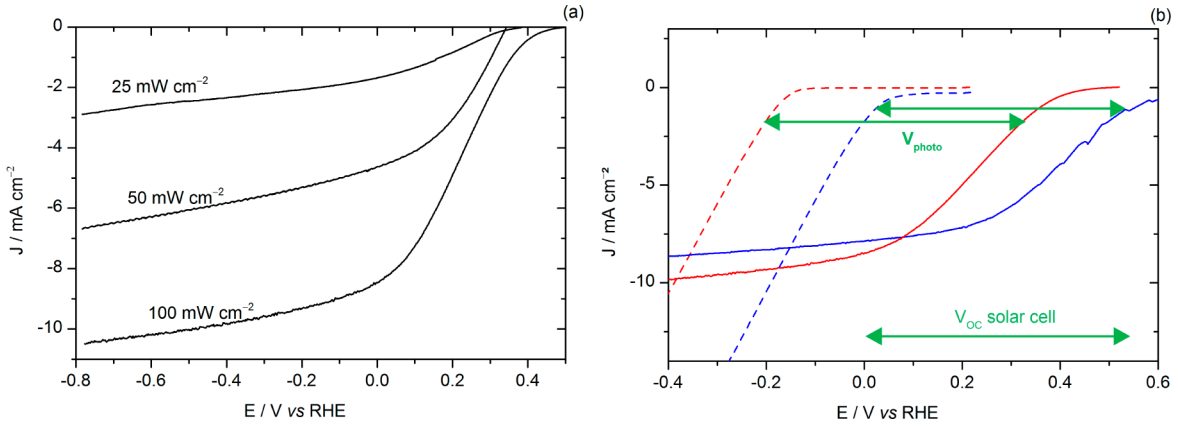

Figure 2. (a) Voltammograms recorded at 50 mV s^{-1} in 0.5 M H_2SO_4 with visible-light illumination for a ITO/PEDOT:PSS/P3HT:PCBM/LiF/Al/Ti−MoS_3 photocathode. The power of the light source was changed from ∼100 to ∼25 mW cm^{-2}. New photocathodes were taken for each test with different power. Electrode area: 0.32 cm^2. (b) Voltammogram recorded at 5 mV s^{-1} in 0.5 M H_2SO_4 for an ITO−MoS_3 cathode (red dotted line) and an ITO−Pt/C cathode (blue dotted line) and at 50 mV s^{-1} with visible-light illumination (100 mW cm^{-2}) for an ITO/PEDOT:PSS/P3HT:PCBM/LiF/Al/Ti−MoS_3 photocathode (red line) and an ITO/PEDOT:PSS/P3HT:PCBM/LiF/Al/Ti−Pt/C photocathode (blue line).

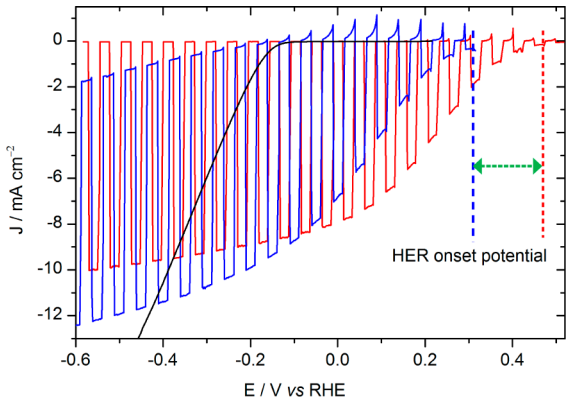

Figure 3. Voltammograms recorded at 50 mV s^{-1} in 0.5 M H_2SO_4 with chopped visible light: (red) ITO/PEDOT:PSS/P3HT:PCBM/LiF/Al/Ti−MoS_3 photocathode (electrode area: 0.32 cm^2); (blue) ITO/PEDOT:PSS/P3HT:PCBM/Ti−MoS_3 (0.28 cm^2). The green arrow represents the shift of the HER onset potential of 150 mV.

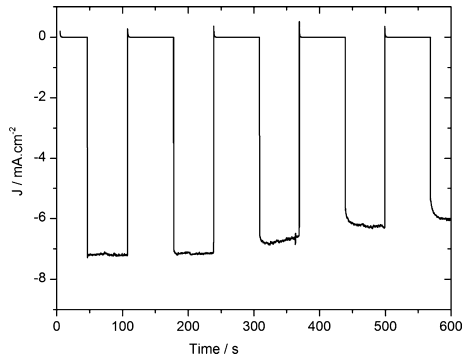

Figure 4. Chronoamperometry at 0 V versus RHE in 0.5 M H_2SO_4 with chopped visible light for an ITO/PEDOT:PSS/P3HT:PCBM/Ti−MoS_3 photocathode (black). Electrode area: 0.28 cm^2.

Ti. However, the HER onset of the new photocathode was 150 mV more negative than the former one containing the LiF/Al layer. Actually the photovoltage provided by the solar cell is limited to 0.45 V (from −0.15 to +0.32 V vs RHE), compared to 0.6 V with LiF/Al/Ti. The lower photovoltage obtained without the LiF/Al layer can be attributed to the difference in the metals work functions (Figure S4 in the SI), which changes the electron injection barrier.

Stability measurements were then performed with chopped light at 0 V versus RHE. The results are presented in Figure 4. The use of titanium as the sole interfacial layer clearly increased the stability under operation, with a loss of only 12% of the photocurrent over 10 min, while the same photocathode with a LiF/Al/Ti interfacial layer was found to lose 45% of its performance under similar conditions (Figure S3 in the SI). Moreover, after 1 h, the Ti layer was not peeled off as the LiF/Al/Ti layer was. Thus, devices made without an Al layer were found to be significantly more stable.

In summary, the use of metallic layers dramatically increased the efficiencies of the photocathodes compared to the first photocathodes that we reported, which displayed photocurrent densities limited to 180 μA cm^{-2}.[25] These interfacial layers bury the P3HT:PCBM layer and electronically separate the catalyst/electrolyte interface and photovoltaic cell. The p/n junction providing the photovoltage and driving force for HER is therefore not directly related to the difference between the redox potential of interest (H^+/H_2) and the conduction band-edge position of the acceptor material (here PCBM). This removes the constraint of their alignment[33] and also explains why the $I-V$ curves obtained with these photocathodes are shaped like the $I-V$ curves of the solar cells: all photogenerated electrons are collected by the metallic layer and then transferred to MoS_3 for catalysis. Because no direct liquid−semiconductor junction is formed, these devices can be identified as part of a PV-biased electrosynthetic cell,[34] which is bringing the device a step away from the direct sensitization of a catalyst, that is, a step closer to a PV electrolyzer.[5] Finding chemically resistant, conductive, and water-tight materials is still a challenging task, but metallic titanium is close to meeting all of the criteria. Indeed, contrary to aluminum, it does not dissolve in acidic water and is conductive. However, in terms of photovoltage, the use of a Ti interfacial layer alone shifts the $J-V$ curve 150 mV more negative than with a combined Ti/Al layer. Then, we decided to test a fully organic interfacial layer by evaporating C_{60}, an n-type OSC typically used in organic PV cells.

3.2. Organic C_{60} Interfacial Layer. C_{60} is an organic molecule with a work function located between PCBM and MoS_3, which makes it suitable as an interfacial material for

DOI: 10.1021/acsami.5b03532
ACS Appl. Mater. Interfaces 2015, 7, 16395−16403

transferring the photogenerated electrons to MoS_3. Deposition of thin layers is well-controlled with the use of vacuum evaporation. A total of 50 nm of C_{60} was evaporated on P3HT:PCBM, and the MoS_3 suspension was then sprayed onto C_{60}. The voltammogram recorded under chopped light is presented in Figure 5.

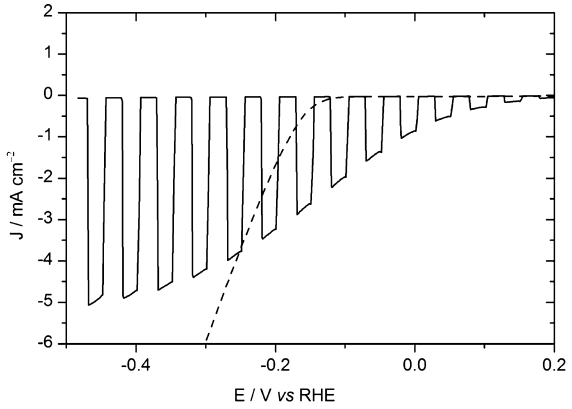

Figure 5. Voltammogram recorded at 50 mV s^{-1} in 0.5 M H_2SO_4 with chopped visible light for an ITO/PEDOT:PSS/P3HT:PCBM/C_{60}–MoS_3 photocathode (electrode area: 0.06 cm^2). The polarization curve of ITO–MoS_3 recorded at 5 mV s^{-1} is shown for comparison (dashed line). Electrode area: 0.28 cm^2.

Compared to our first photocathodes (without any interfacial layers, reaching 180 μA cm^{-2}),[25] the saturation photocurrent density and photovoltage are greatly enhanced. The photocurrent for ITO/PEDOT:PSS/P3HT:PCBM/C_{60}–MoS_3 photocathode is about 1 mA cm^{-2} at 0 V versus RHE (black line in Figure 5) without any metallic interlayer. Again, the onset potential of the HER is shifted in the anodic direction from −0.15 V versus RHE (MoS_3 in the dark) to +0.18 V versus RHE (light-driven HER); i.e., the photosensitizer provides a photovoltage of 0.33 V under operating conditions. The *J*–*V* curves of the ITO/PEDOT:PSS/P3HT:PCBM/C_{60}/LiF/Al solid-state solar cell (Figure S5 in the SI) and of the corresponding ITO/PEDOT:PSS/P3HT:PCBM/C_{60}–MoS_3 photocathode are more different from each other than the ITO/PEDOT:PSS/P3HT:PCBM/LiF/Al solid-state solar cell and the corresponding ITO/PEDOT:PSS/P3HT:PCBM/LiF/Al/Ti–MoS_3 photocathode (Figure 1). Indeed, the current density of the photocathode with C_{60} does not reach the saturation obtained in the corresponding solar cell, while this saturation is reached for the photocathode with the LiF/Al/Ti interfacial layer. This could arise from a higher resistance in electronic transfer from C_{60} to MoS_3 than from Al/Ti to MoS_3 but also from the fact that the ITO/PEDOT:PSS/P3HT:PCBM/C_{60}–MoS_3 photocathode does not benefit from the reflectivity of the metallic layer of the ITO/PEDOT:PSS/P3HT:PCBM/LiF/Al/Ti–MoS_3 photocathode, which enhances the photocurrent density. Moreover, both V_{OC} and J_{SC} of the ITO/PEDOT:PSS/P3HT:PCBM/C_{60}/LiF/Al solid-state solar cell decreased compared to those of the ITO/PEDOT:PSS/P3HT:PCBM/LiF/Al solar cell (Figure S6 in the SI), possibly because of resistive losses due to the limited C_{60} conductivity of about 10^{-7} S cm^{-1}.[35]

The hydrophobic nature of C_{60}[36] was expected to ensure better stability of the underlying P3HT:PCBM layer by preventing water from reaching it. However, Figure 6 shows that the photocathodes based on C_{60} interlayers degrade rapidly. The second scan already shows both a decrease of the photocurrent and a shift of the onset HER potential under irradiation toward more negative potentials, finally stabilizing near the equilibrium potential.

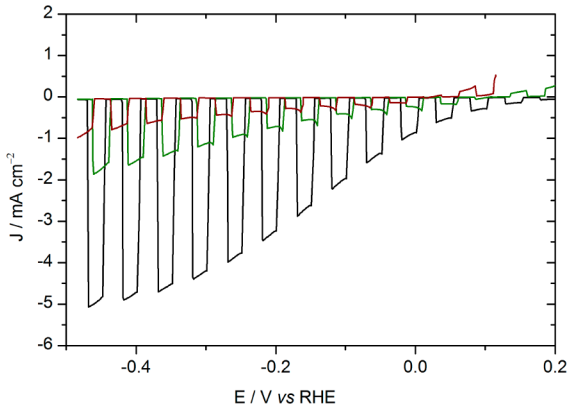

Figure 6. Voltammograms recorded at 50 mV s^{-1} in 0.5 M H_2SO_4 with chopped visible light for the same ITO/PEDOT:PSS/P3HT:PCBM/C_{60}–MoS_3 photocathode: black, first cycle (same as Figure 5); green, second cycle; brown, third cycle. Electrode area: 0.06 cm^2. The oxidation current appearing at anodic potentials was also appearing in configurations without C_{60}: thus, the oxidation current was not attributed to a possible reaction or degradation of C_{60} but more probably to the absence of equilibration time between the measurements.

These results are consistent with the previous results regarding the effect of a layer burying the P3HT:PCBM BHJ in the whole architecture and suppressing the semiconductor/electrolyte interface. During the first cycle, the C_{60} layer does not contain water and partly separates the P3HT:PCBM material from the electrolyte. In the following cycles, the water progressively diffuses into the C_{60} layer and progressively reaches P3HT:PCBM, as if there was no more interfacial layer protecting the device, explaining the shift in the onset HER potential as well as the decrease of the photocurrent. The C_{60} layer increases the photocurrent density at the RHE potential to 1 mA cm^{-2} without any metallic layer. We are now investigating the possibility of depositing more stable C_{60} derivatives using wet deposition processes.

In order to further investigate the impact of the interlayer on the photocathode performances we have carefully analyzed the results by means of two figures-of-merit measuring the amount of power saved by the electrode under operation.

3.3. Comparison of the Photocathode Performance.

The ratiometric power-saved figure-of-merit $\Phi_{saved,ideal}$ (eq 1) relative to RHE, i.e., an ideally nonpolarizable dark electrode for the same reaction, provides information on the ability of a photocathode to achieve H_2 evolution at potentials more positive than the thermodynamic potential of H^+/H_2. Unlike the STH efficiency, which applies for devices achieving overall water splitting assayed in a two-electrode configuration[1,2] (see the SI for details), the ratiometric power-saved figure-of-merit $\Phi_{saved,ideal}$ measures the performance of a single photoelectrode tested under illumination in a three-electrode configuration and is extracted from the maximum power point of its current–voltage curve:[1,2]

$$\Phi_{saved,ideal} = \eta_F \frac{|J_m|[E_{light}(J_m) - E_{RHE}]}{P_{in}} = \eta_F \frac{|J_m|E_{light}^{vs\ RHE}(J_m)}{P_{in}} \quad (1)$$

DOI: 10.1021/acsami.5b03532
ACS Appl. Mater. Interfaces 2015, 7, 16395–16403

The potential is referenced to the thermodynamic potential of the half-reaction (H^+/H_2) at the pH of the electrolyte, i.e., referenced to the RHE, and the current density is in milliampere per square centimeter. $\Phi_{saved,ideal}$ is obtained at the maximum power P_m, where the potential is $E_{light}(J_m)$ and the current density is J_m (Figure 7). P_{in} is the power of the incident illumination in

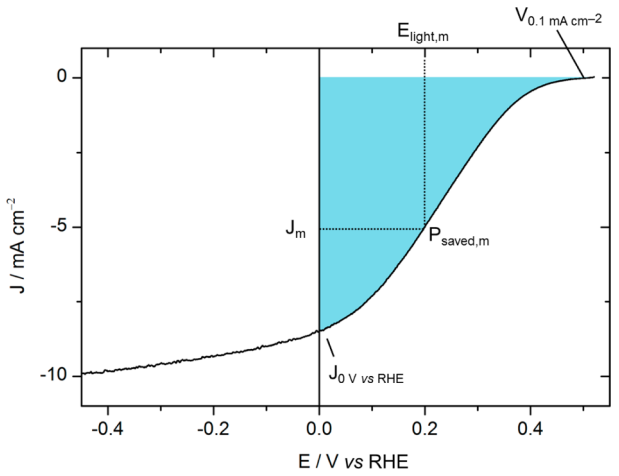

Figure 7. Current density − potential characteristic of an ITO/PEDOT:PSS/P3HT:PCBM/LiF/Al/Ti−MoS_3 photocathode (black line).

milliwatt per square centimeter. The Faradaic efficiency η_F for H_2 evolution is assumed to be 100%, as reported in the literature.[28]

Table 1 presents $\Phi_{saved,ideal}$ for the different photocathodes. The current density at 0 V versus RHE and onset potential

Table 1. $J_{0\ V\ vs\ RHE}$, $V_{0.1\ mA\ cm^{-2}}$, and $\Phi_{saved,ideal}$ of the Different Photocathodes[a]

	$V_{0.1\ mA\ cm^{-2}}$ /V	$J_{0\ V\ vs\ RHE}$/ mA cm^{-2}	$\Phi_{saved,ideal}$/%
ITO/PEDOT:PSS/P3HT:PCBM/ LiF/Al/Ti−MoS_3	0.48	8.47	0.641
ITO/PEDOT:PSS/P3HT:PCBM/ LiF/Al/Ti−Pt/C	0.67	7.87	1.18
ITO/PEDOT:PSS/P3HT:PCBM/ Ti−MoS_3	0.32	6.81	0.241
ITO/PEDOT:PSS/P3HT:PCBM/ C_{60}−MoS_3	0.24	0.86	0.006

[a] $V_{0.1\ mA\ cm^{-2}}$, the onset potential, is the potential necessary to obtain a current density that was arbitrarily chosen at 0.1 mA cm^{-2}, and $J_{0\ V\ vs\ RHE}$ is the current density obtained at the thermodynamic potential. Two different areas were taken into account for $\Phi_{saved,ideal}$ calculation: the current density J_{mp} was multiplied by the electrode area in contact with the electrolyte, while P_{in} was referred to the lightened area (0.5 cm^2) because this area would collect the electrons and transport them to the electrochemical area. If no distinction is made between these two areas, it results in an overestimation of the $\Phi_{saved,ideal}$ value (1.00%, 0.43%, 1.84%, and 0.03%, respectively).

(arbitrarily taken at 0.1 mA cm^{-2}) are also presented for comparison between the cells.

First, for identical absorber and interlayer (ITO/PEDOT:PSS/P3HT:PCBM/LiF/Al/Ti) but with two different catalysts (MoS_3 and Pt/C), the $\Phi_{saved,ideal}$ values are significantly different, equal to 0.64% and 1.18%, respectively. This difference mainly comes from the onset potential that is higher with Pt/C (0.67 V) than with MoS_3 (0.48 V, about 200 mV smaller). This is due to the additional overpotential of MoS_3 to catalyze the HER, as shown in Figure 2b. The short-circuit current is similar to those of both MoS_3 and Pt/C because the saturation current is reached for both photocathodes at a positive potential, but the current at the maximum power point is slightly higher in the case of the Pt/C catalyst because the saturation current is reached before that in the case of the MoS_3 catalyst. For the ITO/PEDOT:PSS/P3HT:PCBM/Ti−MoS_3 photocathode, $\Phi_{saved,ideal}$ is 0.24%, i.e., 2.7 times less than with the same catalyst (MoS_3) but different interlayer (LiF/Al/Ti), because the photocatalytic onset potential is closer to 0 V vs RHE (0.32 V), and the saturation current is not reached at a positive potential. Finally, for the C_{60} interlayer coupled with MoS_3, the onset potential is 0.24 V, close to that with Ti, but $J_{0\ V\ vs\ RHE}$ is much lower, probably because of unsatisfactory electronic transfer between C_{60} and MoS_3, resulting in a slowly increasing HER slope and a small value of $\Phi_{saved,ideal}$ (0.006%).

$\Phi_{saved,ideal}$ depends on the efficiency of both the photoproduction of charges in P3HT:PCBM and their utilization by the catalyst, which are not differentiated in this figure-of-merit. It may thus be interesting to consider another quantity, which is less catalyst-dependent: the power-saved metric relative to a nonphotoactive dark electrode with an identical catalyst and measured in an identical three-electrode electrochemical cell

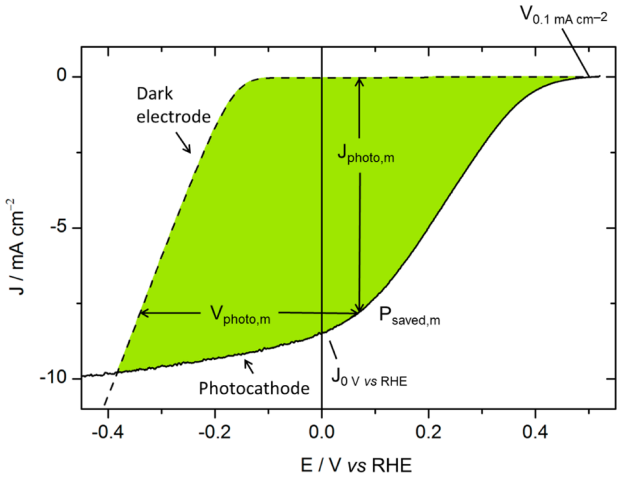

Figure 8. Current density − potential characteristic of an ITO/PEDOT:PSS/P3HT:PCBM/LiF/Al/Ti−MoS_3 photocathode (black line) and of an ITO−MoS_3 dark cathode (black dashed line). The photovoltage at a given current is thus evaluated from the potential under illumination compared to that of the same catalyst directly deposited on ITO.

(Figure 8). $\Phi_{saved,NPAC}$ (NPAC = nonphotoactive, identical catalyst) is calculated following eq 2:[1]

$$\Phi_{saved,NPAC} = \eta_F \frac{|J_{photo,m}|[E_{light}(J_{photo,m}) - E_{dark}(J_{photo,m})]}{P_{in}} = \eta_F \frac{|J_{photo,m}|V_{photo,m}}{P_{in}} \quad (2)$$

where η_F is the Faradaic efficiency assumed to be 100% again, P_{in} is the power of the incident illumination, and $J_{photo,m}$ and $V_{photo,m}$ are the photocurrent and photovoltage at the maximum power point.

For the comparison of a photoelectrode, $\Phi_{saved,ideal}$ and $\Phi_{saved,NPAC}$ are both important values because $\Phi_{saved,ideal}$ reflects

DOI: 10.1021/acsami.5b03532
ACS Appl. Mater. Interfaces 2015, 7, 16395−16403

Table 2. For Different Photocathodes Measured at 100 mW cm^{-2}: $\Phi_{saved,ideal}$ and $\Phi_{saved,NPAC}$ at Maximum Power Point with Their Corresponding Current Density and Potential (J_{mp} and V_{mp}, $J_{photo,mp}$ and $V_{photo,mp}$)[a]

	$\Phi_{saved,ideal}$	$\Phi_{saved,NPAC}$
ITO/PEDOT:PSS/P3HT:PCBM/LiF/Al/Ti−MoS_3	0.64% (J_m = 5.1 mA cm^{-2}, V_m = 0.20 V)	2.05% ($J_{photo,m}$ = 7.8 mA cm^{-2}, $V_{photo,m}$ = 0.41 V)
ITO/PEDOT:PSS/P3HT:PCBM/LiF/Al/Ti−Pt/C	1.42% (J_m = 6.0 mA cm^{-2}, V_m = 0.31 V)	1.64% ($J_{photo,m}$ = 6.7 mA cm^{-2}, $V_{photo,m}$ = 0.39 V)
ITO/PEDOT:PSS/P3HT:PCBM/Ti−MoS_3	0.24% (J_m = 3.9 mA cm^{-2}, V_m = 0.11 V)	1.30% ($J_{photo,m}$ = 7.7 mA cm^{-2}, $V_{photo,m}$ = 0.30 V)
ITO/PEDOT:PSS/P3HT:PCBM/C_{60}−MoS_3	0.006% (J_m = 0.4 mA cm^{-2}, V_m = 0.008 V)	0.14% ($J_{photo,m}$ = 2.1 mA cm^{-2}, $V_{photo,m}$ = 0.30 V)

[a]Table S1 in the SI gathers all data of Tables 1 and 2, as well as the calculation for ITO/PEDOT:PSS/P3HT:PCBM/LiF/Al/Ti−MoS_3 at different incident power. As for Table 1, two different areas were taken into account: the current density $J_{photo,mp}$ was multiplied by the electrode area in contact with the electrolyte, while P_{in} was referred to the lightened area (0.5 cm^2).

the optimum power point for the use of the photoelectrode in practical applications (i.e., depending on the performance of both the photovoltaic material and catalyst), while $\Phi_{saved,NPAC}$ reflects the photovoltage and photocurrent of a photocathode independently from the overpotential requirement of the catalyst.

Some details of the procedure to calculate $\Phi_{saved,NPAC}$ are presented in the SI. Figure S7 shows the curves used in the case of the MoS_3 catalyst and the LiF/Al/Ti interfacial layer. The photocurrent J_{photo} is the difference between the current under illumination (J_{light}, i.e., measured for the ITO/PEDOT:PSS/P3HT:PCBM/LiF/Al/Ti−MoS_3 photocathode) and of the catalyst (J_{dark}, measured for ITO−MoS_3). As expected, J_{photo} increases at the same rate as J_{light} when the voltage is swept in the cathodic direction. Once the onset of the HER of the catalyst is reached, J_{photo} decreases with an increase of J_{dark}. From these data, the photovoltage V_{photo} is obtained by subtracting U_{dark} from U_{light} at matching current densities. J_{photo} as a function of V_{photo} is shown in Figure S8 in the SI (right, Y axis).

Table 2 presents $\Phi_{saved,ideal}$ and $\Phi_{saved,ideal}$ as well as the photovoltages and photocurrents in each case.

First, $\Phi_{saved,NPAC}$ and $\Phi_{saved,ideal}$ for the same system with LiF/Al/Ti as the interlayer and MoS_3 as the catalyst are significantly different: $\Phi_{saved,NPAC}$ (2.05%) is 3.2 times larger than $\Phi_{saved,ideal}$ (0.64%). This higher $\Phi_{saved,NPAC}$ is due to both a higher photovoltage and a higher photocurrent at which the maximum power point is obtained: $V_{photo,m}$ is 0.41 V, while V_m is only 0.2 V. This 0.21 V loss is a consequence of the overpotential requirement of the catalyst, and in the photocathode, a significant part of the photovoltage is thus used to overcome the overpotential requirement of MoS_3 to mediate HER. Moreover, the photocurrent $J_{photo,m}$ (7.8 mA cm^{-2}) is 50% larger than J_m (5.1 mA cm^{-2}) because the saturation photocurrent is barely reached at positive potentials (toward the RHE). On the contrary, with the Pt/C catalyst (ITO/PEDOT:PSS/P3HT:PCBM/LiF/Al/Ti−Pt/C photocathode), which mediates HER at much lower overpotential values than MoS_3, the difference between the two figures-of-merit is much less: $\Phi_{saved,NPAC}$ (1.64%) is only 1.2 times $\Phi_{saved,ideal}$ (1.42%) because the photovoltage does not need to be used for overcoming the overpotential of the catalyst (V_m and $V_{photo,m}$ are 0.31 and 0.39 V, respectively).

In a next step, $\Phi_{saved,NPAC}$ and $\Phi_{saved,ideal}$ can be compared for two photocathodes with different catalysts (Pt/C and MoS_3) but with identical interfacial layers (LiF/Al/Ti). In this case, $\Phi_{saved,NPAC}$ with MoS_3 and with Pt (2.05% and 1.64%) are closer than $\Phi_{saved,ideal}$ (0.64% and 1.42%) because the maximum photovoltages in both photocathodes are similar (0.41 and 0.39 V), as well as the maximum photocurrent densities (7.8 and 6.7 mA cm^{-2}). Thus, $\Phi_{saved,NPAC}$ is independent of the catalyst performance and is a suitable figure-of-merit for the comparison of different light-harvesting modules. It is illustrated by the ITO/PEDOT:PSS/P3HT:PCBM/Ti−MoS_3 photocathode, whose $\Phi_{saved,NPAC}$ is 1.3%, i.e., 1.6 times less than with the LiF/Al/Ti interfacial layer (2.05%) with identical catalysts (MoS_3). It shows that the lower efficiency obtained with the Ti layer is due to the light-harvesting part and not to the catalyst overpotential requirement. This effect is even more pronounced with the C_{60} interlayer.

4. CONCLUSION

Photocathodes based on P3HT:PCBM solar cells and a noble-metal-free catalyst, MoS_3, evolve H_2 at the RHE potential thanks to the introduction of interfacial layers, which improved the charge transfer from the photocathode to the catalyst mediating proton reduction. Moreover, these interfacial layers bury the P3HT:PCBM p/n junction, removing the constraint of energy level alignment between the redox potential of interest (H^+/H_2) and the conduction band-edge position of the acceptor material (here PCBM).

The organic cell provides a photovoltage of 0.6 V, which is close to the open-circuit potential measured in solid-state devices when the metallic LiF/Al/Ti layer is used, while the photocurrent at the RHE potential reaches 8 mA cm^{-2}, corresponding to a value of ratiometric saved power of 2.05%. Increased stability is obtained by using only Ti as the interfacial layer, although it results in a ratiometric saved power value of 1.30% due to a 150 mV cathodic shift of the $J-V$ curve. The photovoltage and photocurrent are lower in the case of C_{60}, probably because of resistive losses appearing at the interfaces. As described in a recent work,[37] TiO_x layers also work as efficient interfacial layers in this context in combination with Pt as the HER catalyst. Using other types of organic and polymeric photovoltaic materials delivering a higher V_{OC}, e.g., PCDTBT (poly[*N*-9′-heptadecanyl-2,7-carbazole-*alt*-5,5-(4,7-di-2-thienyl)-2′,1′,3′-benzothiadiazole]),[38] the photovoltage values could be further increased. These promising results show that a rational improvement of the performances of such organic solar-cell-based photoelectrodes is possible through the combination of interfacial layers, catalysts, and OSC materials. The stability of the interfacial layers and, consequently, of the devices must be further improved for their integration into practical application, so that further steps will include the search for a novel formulation allowing more durable protection of the photoactive components against corrosion and integration of multijunction organic solar cells.

■ ASSOCIATED CONTENT

Supporting Information

Details of experimental procedures, supplementary figures (Figure S1−S6), STH efficiency (Table S1), and ratiometric power-saved figures-of-merit (Figures S7 and S8). The Supporting Information is available free of charge on the ACS Publications website at DOI: 10.1021/acsami.5b03532.

DOI: 10.1021/acsami.5b03532
ACS Appl. Mater. Interfaces 2015, 7, 16395−16403

AUTHOR INFORMATION

Corresponding Author

*E-mail: bruno.jousselme@cea.fr.

Notes

The authors declare no competing financial interest.

ACKNOWLEDGMENTS

We are indebted to the CEA for financial support through the DSM Energy Program for the Ph.D. thesis grant assigned to R.B. This work was partially supported by the French National Research Agency (Labex program, ARCANE, ANR-11-LABX-0003-01) and the European Research Council under the European Union's Seventh Framework Programme (FP/2007-2013)/ERC Grant Agreement 306398.

REFERENCES

(1) Coridan, R. H.; Nielander, A. C.; Francis, S. A.; McDowell, M. T.; Dix, V.; Chatman, S. M.; Lewis, N. S. Methods for Comparing the Performance of Energy-Conversion Systems for Use in Solar Fuels and Solar Electricity Generation. *Energy Environ. Sci.* **2015**, DOI: 10.1039/C5EE00777A.

(2) Walter, M. G.; Warren, E. L.; McKone, J. R.; Boettcher, S. W.; Mi, Q.; Santori, E. A.; Lewis, N. S. Solar Water Splitting Cells. *Chem. Rev.* **2010**, *110* (11), 6446−6473.

(3) Li, Z.; Luo, W.; Zhang, M.; Feng, J.; Zou, Z. Photoelectrochemical Cells for Solar Hydrogen Production: Current State of Promising Photoelectrodes, Methods to Improve Their Properties, and Outlook. *Energy Environ. Sci.* **2013**, *6* (2), 347−370.

(4) Protti, S.; Albini, A.; Serpone, N. Photocatalytic Generation of Solar Fuels from the Reduction of H_2O and CO_2: A Look at the Patent Literature. *Phys. Chem. Chem. Phys.* **2014**, *16* (37), 19790−19827.

(5) Jacobsson, T. J.; Fjällström, V.; Edoff, M.; Edvinsson, T. Sustainable Solar Hydrogen Production: From Photoelectrochemical Cells to PV-Electrolyzers and Back Again. *Energy Environ. Sci.* **2014**, *7*, 2056−2070.

(6) Lanzarini, E.; Antognazza, M. R.; Biso, M.; Ansaldo, A.; Laudato, L.; Bruno, P.; Metrangolo, P.; Resnati, G.; Ricci, D.; Lanzani, G. Polymer-Based Photocatalytic Hydrogen Generation. *J. Phys. Chem. C* **2012**, *116* (20), 10944−10949.

(7) Krebs, F. C.; Hösel, M.; Corazza, M.; Roth, B.; Madsen, M. V.; Gevorgyan, S. A.; Søndergaard, R. R.; Karg, D.; Jørgensen, M. Freely Available OPV - The Fast Way to Progress. *Energy Technol.* **2013**, *1* (7), 378−381.

(8) Licht, S.; Wang, B.; Mukerji, S.; Soga, T.; Umeno, M.; Tributsch, H. Over 18% Solar Energy Conversion to Generation of Hydrogen Fuel; Theory and Experiment for Efficient Solar Water Splitting. *Int. J. Hydrogen Energy* **2001**, *26*, 653−659.

(9) Rocheleau, R. E.; Miller, E. L.; Misra, A. High-Efficiency Photoelectrochemical Hydrogen Production Using Multijunction Amorphous Silicon Photoelectrodes. *Energy Fuels* **1998**, *12* (1), 3−10.

(10) Yamada, Y.; Matsuki, N.; Ohmori, T.; Mametsuka, H.; Kondo, M.; Matsuda, A.; Suzuki, E. One Chip Photovoltaic Water Electrolysis Device. *Int. J. Hydrogen Energy* **2003**, *28* (11), 1167−1169.

(11) Reece, S. Y.; Hamel, J. A.; Sung, K.; Jarvi, T. D.; Esswein, A. J.; Pijpers, J. J. H.; Nocera, D. G. Wireless Solar Water Splitting Using Silicon-Based Semiconductors and Earth-Abundant Catalysts. *Science* **2011**, *334*, 645−649.

(12) Morales-Guio, C. G.; Tilley, S. D.; Vrubel, H.; Grätzel, M.; Hu, X. Hydrogen Evolution from a Copper(I) Oxide Photocathode Coated with an Amorphous Molybdenum Sulphide Catalyst. *Nat. Commun.* **2014**, *5*, 3059.

(13) Lin, C.-Y.; Lai, Y.-H.; Mersch, D.; Reisner, E. $Cu_2O|NiO_x$ Nanocomposite as an Inexpensive Photocathode in Photoelectrochemical Water Splitting. *Chem. Sci.* **2012**, *3* (12), 3482−3487.

(14) Park, Y.; McDonald, K. J.; Choi, K.-S. Progress in Bismuth Vanadate Photoanodes for Use in Solar Water Oxidation. *Chem. Soc. Rev.* **2013**, *42*, 2321−2337.

(15) Abdi, F. F.; Han, L.; Smets, A. H. M.; Zeman, M.; Dam, B.; van de Krol, R. Efficient Solar Water Splitting by Enhanced Charge Separation in a Bismuth Vanadate-Silicon Tandem Photoelectrode. *Nat. Commun.* **2013**, *4*, 2195.

(16) Green, M. A.; Emery, K.; Hishikawa, Y.; Warta, W.; Dunlop, E. D. Solar Cell Efficiency Tables (version 45). *Prog. Photovoltaics* **2015**, *23*, 1−9.

(17) Li, W.; Furlan, A.; Hendriks, K. H.; Wienk, M. M.; Janssen, R. A. J. Efficient Tandem and Triple-Junction Polymer Solar Cells. *J. Am. Chem. Soc.* **2013**, *135* (15), 5529−5532.

(18) Chen, S. N.; Heeger, A. J.; Kiss, Z.; MacDiarmid, A. G.; Gau, S. C.; Peebles, D. L. Polyacetylene, $(CH)_x$: Photoelectrochemical Solar Cell. *Appl. Phys. Lett.* **1980**, *36* (1), 96−98.

(19) Yanagida, S.; Kabumoto, A.; Mizumoto, K.; Pac, C.; Yoshino, K. Poly(p-Phenylene)-Catalysed Photoreduction of Water to Hydrogen. *J. Chem. Soc., Chem. Commun.* **1985**, 474−475.

(20) El-Rashiedy, O. A.; Holdcroft, S. Photoelectrochemical Properties of Poly (3-Alkylthiophene) Films in Aqueous Solution. *J. Phys. Chem.* **1996**, *100*, 5481−5484.

(21) Abe, T.; Nagai, K. Novel Photofunctions of Bilayer Composed of P-Type Phthalocyanine and N-Type Organic Semiconductor as Photoelectrodes in the Water Phase. *Org. Electron.* **2007**, *8* (2−3), 262−271.

(22) Suppes, G.; Ballard, E.; Holdcroft, S. Aqueous Photocathode Activity of Regioregular poly(3-Hexylthiophene). *Polym. Chem.* **2013**, *4* (20), 5345−5250.

(23) Abe, T.; Tobinai, S.; Taira, N.; Chiba, J.; Itoh, T.; Nagai, K. Molecular Hydrogen Evolution by Organic p/n Bilayer Film of Phthalocyanine/Fullerene in the Entire Visible-Light Energy Region. *J. Phys. Chem. C* **2011**, *115* (15), 7701−7705.

(24) Lattach, Y.; Fortage, J.; Deronzier, A.; Moutet, J.-C. Polypyrrole-$Ru(2,2'\text{-bipyridine})_3^{2+}/MoS_x$ Structured Composite Film As a Photocathode for the Hydrogen Evolution Reaction. *ACS Appl. Mater. Interfaces* **2015**, *7* (8), 4476−4480.

(25) Bourgeteau, T.; Tondelier, D.; Geffroy, B.; Brisse, R.; Laberty-Robert, C.; Campidelli, S.; de Bettignies, R.; Artero, V.; Palacin, S.; Jousselme, B. A H_2-Evolving Photocathode Based on Direct Sensitization of MoS_3 with an Organic Photovoltaic Cell. *Energy Environ. Sci.* **2013**, *6* (9), 2706−2713.

(26) Morales-Guio, C. G.; Hu, X. Amorphous Molybdenum Sulfides as Hydrogen Evolution Catalysts. *Acc. Chem. Res.* **2014**, *47* (8), 2671−2681.

(27) Guerrero, A.; Haro, M.; Bellani, S.; Antognazza, M. R.; Meda, L.; Gimenez, S.; Bisquert, J. Organic Photoelectrochemical Cells with Quantitative Photocarrier Conversion. *Energy Environ. Sci.* **2014**, *7* (11), 3666−3673.

(28) Vrubel, H.; Merki, D.; Hu, X. Hydrogen Evolution Catalyzed by MoS_3 and MoS_2 Particles. *Energy Environ. Sci.* **2012**, *5* (3), 6136−6144.

(29) Seger, B.; Laursen, A. B.; Vesborg, P. C. K.; Pedersen, T.; Hansen, O.; Dahl, S.; Chorkendorff, I. Hydrogen Production Using a Molybdenum Sulfide Catalyst on a Titanium-Protected n^+p-Silicon Photocathode. *Angew. Chem., Int. Ed.* **2012**, *51* (36), 9128−9131.

(30) Seger, B.; Pedersen, T.; Laursen, A. B.; Vesborg, P. C. K.; Hansen, O.; Chorkendorff, I. Using TiO_2 as a Conductive Protective Layer for Photocathodic H_2 Evolution. *J. Am. Chem. Soc.* **2013**, *135* (3), 1057−1064.

(31) Seger, B.; Tilley, S. D.; Pedersen, T.; Vesborg, P. C. K.; Hansen, O.; Grätzel, M.; Chorkendorff, I. Silicon Protected with Atomic Layer Deposited TiO_2: Conducting versus Tunnelling through TiO_2. *J. Mater. Chem. A* **2013**, *1* (47), 15089−15094.

(32) Seger, B.; Tilley, D. S.; Pedersen, T.; Vesborg, P. C. K.; Hansen, O.; Grätzel, M.; Chorkendorff, I. Silicon Protected with Atomic Layer Deposited TiO_2: Durability Studies of Photocathodic H_2 Evolution. *RSC Adv.* **2013**, *3* (48), 25902−25907.

(33) Jacobsson, T. J.; Fjällström, V.; Sahlberg, M.; Edoff, M.; Edvinsson, T. A Monolithic Device for Solar Water Splitting Based on Series Interconnected Thin Film Absorbers Reaching over 10% Solar-to-Hydrogen Efficiency. *Energy Environ. Sci.* **2013**, *6* (12), 3676−3683.

DOI: 10.1021/acsami.5b03532
ACS Appl. Mater. Interfaces 2015, 7, 16395−16403

(34) Nielander, A. C.; Shaner, M. R.; Papadantonakis, K. M.; Francis, S. A.; Lewis, N. S. A Taxonomy for Solar Fuels Generators. *Energy Environ. Sci.* **2015**, *8* (1), 16−25.
(35) Rikitake, K.; Akiyama, T.; Takashima, W.; Kaneto, K. Relationships between Crystallinity and Conductivity in Evaporated C_{60} Films. *Synth. Met.* **1997**, *86*, 2357−2358.
(36) Labille, J.; Brant, J.; Villiéras, F.; Pelletier, M.; Thill, A.; Masion, A.; Wiesner, M.; Rose, J.; Bottero, J.-Y. Affinity of C_{60} Fullerenes with Water. *Fullerenes, Nanotubes, Carbon Nanostruct.* **2006**, *14* (2−3), 307−314.
(37) Haro, M.; Solis, C.; Molina, G.; Otero, L.; Bisquert, J.; Gimenez, S.; Guerrero, A. Towards Stable Solar Hydrogen Generation Using Organic Photoelectrochemical Cells. *J. Phys. Chem. C* **2015**, *119* (12), 6488−6494.
(38) Park, S. H.; Roy, A.; Beaupré, S.; Cho, S.; Coates, N.; Moon, J. S.; Moses, D.; Leclerc, M.; Lee, K.; Heeger, A. J. Bulk Heterojunction Solar Cells with Internal Quantum Efficiency Approaching 100%. *Nat. Photonics* **2009**, *3* (5), 297−302.

DOI: 10.1021/acsami.5b03532
ACS Appl. Mater. Interfaces 2015, 7, 16395−16403